JOC The Journal of Organic Chemistry

Article

pubs.acs.org/joc

Coumarin- and Rhodamine-Fused Deep Red Fluorescent Dyes: Synthesis, Photophysical Properties, and Bioimaging in Vitro

Jianhong Chen,[†,‡] Weimin Liu,*[,†] Bingjiang Zhou,[†,‡] Guangle Niu,[†,‡] Hongyan Zhang,[†] Jiasheng Wu,[†] Ying Wang,[†] Weigang Ju,[†] and Pengfei Wang*[,†]

[†]Key Laboratory of Photochemical Conversion and Optoelectronic Materials, Technical Institute of Physics and Chemistry, Chinese Academy of Sciences, Beijing 100190, China

[‡]University of Chinese Academy of Sciences, Beijing 100049, China

Supporting Information

ABSTRACT: A series of deep red fluorescent dyes (**CR1** to **CR3**) was developed via introduction of a coumarin moiety into the rhodamine molecular skeleton. The novel dyes possessed the individual advantages of coumarin and rhodamine derivatives, and the emission wavelength was extended to the deep red region (>650 nm) due to the extension of fused-ring conjugate structure simultaneously. To illustrate its value, we designed and conveniently synthesized a series of novel deep red bioimaging dyes (**CR1E** to **CR3E**) by esterification of **CR1** to **CR3**, which could selectively stain mitochondria. They were superior to the MitoTrackers for mitochondrial staining in terms of large Stokes shift, excellent contrast for imaging, high photostability, and low cytotoxicity. Furthermore, the fluorescence of the coumarin moiety and rhodamine-like fluorophore could be switched like classical rhodamine. Thus, they could be used as an effective platform in constructing fluorescence sensors. Based on this fact, we constructed a novel ratiometric sensor (**CR1S**) for Hg^{2+} with good selectivity that could be successfully applied to the imaging of Hg^{2+} in living A549 cells. This design strategy is straightforward and adaptable to various deep red dyes and sensing platforms by simply introducing different fluorophores.

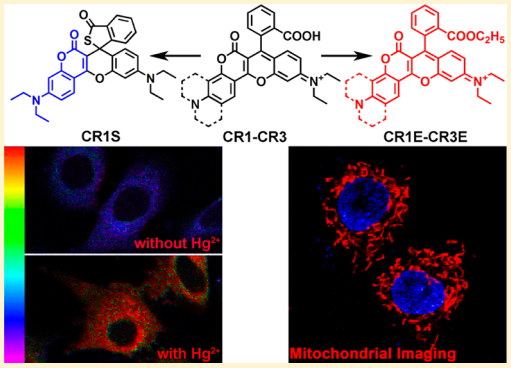

INTRODUCTION

On the basis of the virtue of its highly sensitive and high-speed spatial analysis of cells, fluorescence bioimaging has become a facile and powerful tool for visualizing morphological details and monitoring biomolecules in living systems.[1] This imaging technique is highly dependent on the photophysical and photochemical properties of the applied fluorescent dyes. Among the commonly used fluorescent dyes, rhodamine derivatives are highly favored in bioimaging and biosensors because of their excellent photophysical properties, such as high molar extinction coefficients, excellent fluorescence quantum yields, and great photostability.[2] For example, Rhodamine 123 has been described to selectively sequester in active mitochondria and used as a marker for mitochondrial membrane potentials (MMP).[3] In addition, rhodamine derivatives can undergo equilibrium between spirocyclic and open-ring forms. The spirocyclic forms of these dyes are colorless and nonfluorescent due to the small π-conjugated systems, while the open-ring forms show intensive spectroscopic signals in the absorption and fluorescence spectra by generating the large π-conjutated systems.[4] Thus, they can be used as an effective platform based on spirocyclic/open-ring switching mechanism in constructing fluorescence turn-on sensors for heavy metal ions and biomolecules.[1a,2,4,5]

However, most rhodamine-based sensors only show a single emission, which is perturbed by environmental factors, such as sensor molecular concentration, pH, temperature, solvent polarity, and so on.[6] To eliminate these influences, ratio measurements are favorable because the simultaneous observation of the absorption or emission intensities at two different wavelengths can increase the selectivity and sensitivity. Thus, many rhodamine sensors based on fluorescence resonance energy transfer (FRET) have been designed by introducing the additional fluorophore as a donor, such as naphthalimine, dansyl, coumarin, fluorescein, or BODIPY derivatives.[6] The FRET process will occur only when there is a substantial overlap between the donor emission spectrum and the acceptor absorption spectrum. In addition, the emission of this energy transfer system is still confined to the characteristic emission band of the acceptor (rhodamine; <600 nm).

In contrast to visible and above all ultraviolet, fluorescence imaging with deep red light is advantageous because of its minimum photodamage to biological samples, deep tissue penetration, and negligible interference from the background autofluorescence of biomolecules in the organism.[7] Recently, several studies have aimed at obtaining long wavelength dyes.[1a] These efforts include the extension of the conjugate system[2b,7a,8] and the introduction of donor and acceptor groups into the chromophore,[9] as well as the replacement of the oxygen bridge

Received: April 13, 2013
Published: May 24, 2013

dx.doi.org/10.1021/jo400783x | J. Org. Chem. 2013, 78, 6121−6130

atom of rhodamine derivatives by other elements.[2b,10] However, there are some disadvantages to these methods including their difficult synthesis, chemical instability, and/or high sensitivity to photobleaching. Moreover, rhodamine derivatives exhibit a very small Stokes shift (rhodamine B: 19 nm vs 600 cm^{-1}).[7a] The large Stokes shift could reduce self-absorption as well as obtain high resolution and low detection limits. Therefore, it remains highly desirable to explore new design strategies for the development of deep red fluorescent dye with great photostability and large Stokes shift while being used as ratiometric sensing platforms.

In this work, we constructed a series of novel deep red fluorescent dyes by hybridizing coumarin and rhodamine moieties (**CR1**, **CR2**, and **CR3**, Scheme 1). The new dyes not

Scheme 1. Structural Changes of CR1 to CR3 between Spirocyclic and Open-Ring forms

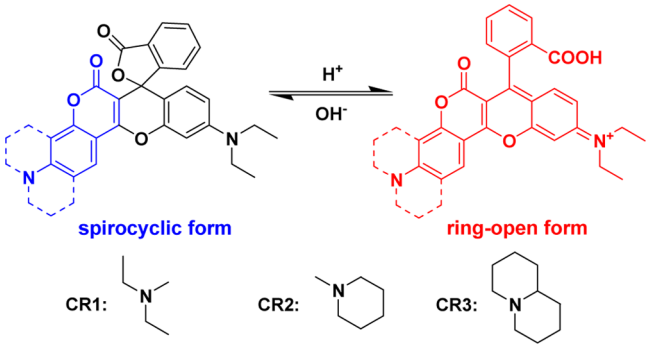

only retained the advantages of coumarin and rhodamine derivatives themselves but also demonstrated the following expected advantages: (i) the emission wavelength was extended to the deep red region (>650 nm in H_2O) when the fused-ring conjugate structure was extended during its facile synthesis; (ii) the fluorescence of the coumarin moiety and rhodamine-like fluorophore was switched by the spirocyclic/open-ring process of the carboxylic acid functional group (−COOH) at the 2′-position. Considering their good photophysical properties, these deep red fluorescent dyes were promising candidates for biological applications, such as biosensor, biomarker, and bioimaging. Based on these new dyes, we first developed deep red mitochondria-specific fluorescent dyes (**CR1E**, **CR2E**, and **CR3E**). Cell-imaging experiments indicated that these dyes were superior over MitoTrackers because of their deep red emission with large Stokes shift, excellent contrast for imaging, high photostability, and low cytotoxicity. To illustrate its value as a ratiometric platform, we further constructed a ratiometric sensor for Hg^{2+} (**CR1S**) with good selectivity and "turn-on" response in the deep red region which was different from all previously reported rhodamine-based FRET systems.

RESULTS AND DISCUSSION

Design and Synthesis. The absorption and emission wavelengths of traditional coumarin dyes were highly dependent on the substituents of the amino group because of intramolecular charge-transfer (ICT) character. Thus, the coumarin- and rhodamine-fused compounds **CR1** to **CR3** were designed using different amino substituents. The detailed synthetic routes and methods are shown in Scheme 2. Compounds **CR1** to **CR3** were synthesized from 3-alkylaminophenol in two steps. Compounds **1**, **2**, **3**, **8**, and **9** were commercially available. Compound **2** was added to 85% phosphoric acid and heated to reflux for 24 h to obtain compound **5**. The condensation of compounds **1** and **8** in toluene for 4 h afforded the intermediate **4**, which was heated to reflux with compound **9** in 1,1,2,2-tetrachloroethane with P_2O_5 for 4 h to produce **CR1**. Similar synthetic pathways were used to synthesize **CR2** and **CR3**.

To demonstrate their properties as fluorescent bioimaging agents, we designed a series of deep red fluorescent dyes (**CR1E** to **CR3E**) by esterification of **CR1** to **CR3** in ethanol with concentrated H_2SO_4 for 2 h, which can selectively stain mitochondria. Mitochondria function as the "powerhouses" of cells by generating ATP through oxidative phosphorylation.[11] These organelles are related to several diseases, ranging from metabolic disorders to cancer.[11c,12] The mitochondria of cancer cells are structurally and functionally different from their normal counterparts. To understand the cellular processes and molecular mechanisms of mitochondrial function, several fluorescent dyes have been developed to selectively stain mitochondria by electrostatic interactions due to its highly negative MMP (about −180 mV).[13] For example, lipophilic and positively charged dyes, such as Rhodamine 123[3] and MitoTracker Red CMXRos (MTR),[14] can selectively accumulate in mitochondria. However, most of these dyes are limited to wavelengths below 600 nm and have small Stokes shift or poor photostability. Compound **CR1E** to **CR3E** demonstrated the long wavelength emissions in the deep red region and large Stokes shift due to the ICT of the coumarin moiety.

In these new dyes, the fluorescence of the coumarin moiety and rhodamine-like fluorophore could be switched like classical rhodamine. Different from all previously reported rhodamine-based sensing systems, these dyes **CR1** to **CR3** have the advantage of deep red emission and a very large Stokes shift. To validate our molecular design strategy, we developed a ratiometric sensor (**CR1S**) for Hg^{2+} based on the well-known desulfurization reaction, which can be used in fluorescence imaging of Hg^{2+} in the living A549 (human lung adenocarcinoma apithelial) cells. Compound **CR1S** was synthesized from **CR1** which was heated to reflux with $POCl_3$ in 1,2-dichloroethane for 4 h and then reacted with saturated Na_2S.[15] Details of the synthesis are given in the Experimental Section. The structures of the intermediate compounds (**4**−**7**) and their respective products (**CR1** to **CR3**, **CR1E** to **CR3E** and **CR1S**) were characterized by ^1H NMR, ^{13}C NMR, and HRMS.

X-ray Structures. The molecular structures of **CR2**, **CR3**, **CR2E**, **CR3E**, and **CR1S** were elucidated by X-ray crystallography, which confirmed a coumarin- and rhodamine-fused skeleton. Single crystals of compounds **CR2**, **CR3**, **CR2E**, **CR3E**, and **CR1S** suitable for X-ray crystallographic analysis were obtained by slow evaporation of CH_3OH and H_2O solutions of the compounds at ambient temperature. Details of X-ray experimental conditions, cell data, and refinement data of **CR2**, **CR3**, **CR2E**, **CR3E**, and **CR1S** are summarized in Table S1 (Supporting Information). These compounds were all racemic mixtures, given the helix structure and the presence of both enantiomers in unit cells. Compounds **CR2**, **CR3**, **CR2E**, and **CR3E** formed a monoclinic unit cell and the $P2(1)/n$ space group, whereas **CR1S** formed a triclinic unit cell and the P-1 space group. The **CR2** and **CR3** crystals were observed capturing one water molecule in the crystal lattice with IHB (Figure 1). The water molecule was located between the dye and perchlorate. The lengths and angles of the IHB were presented in Table 1. The IHB between the dye and water molecule was stronger than that between the water molecule and perchlorate. For example,

dx.doi.org/10.1021/jo400783x | J. Org. Chem. 2013, 78, 6121−6130

Scheme 2. Synthesis of Deep Red Dyes CR1 to CR3 and CR1E to CR3E and the Ratiometric Sensor CR1S[a]

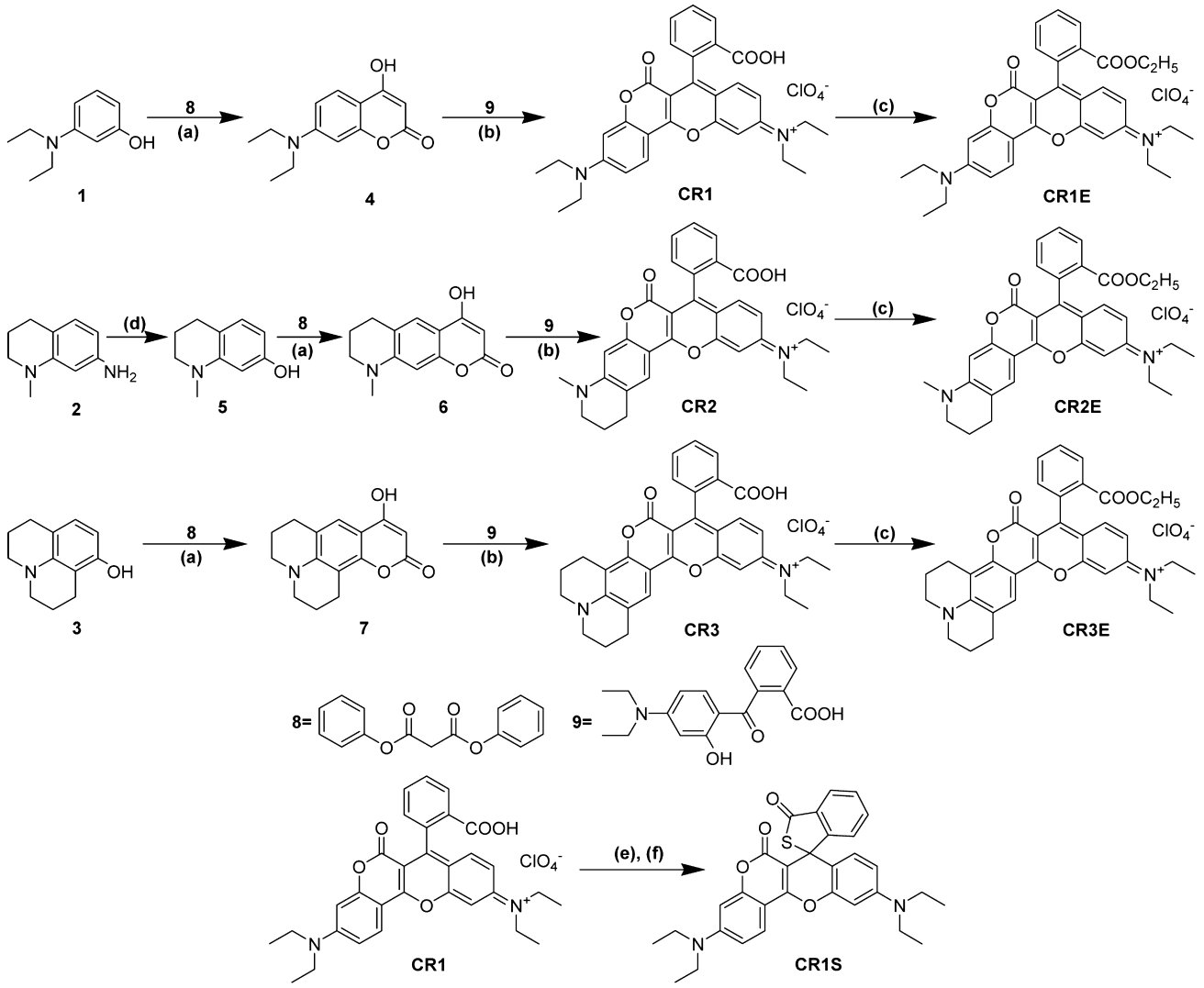

[a]Conditions: (a) toluene, reflux, 4 h; (b) P_2O_5, 1,1,2,2-tetrachloroethane, reflux, 4 h; (c) C_2H_5OH, H_2SO_4, reflux, 2 h; (d) 85% phosphoric acid, reflux, 24 h; (e) $POCl_3$, $ClCH_2CH_2Cl$, reflux, 4 h; (f) excess Na_2S saturated aqueous solution.

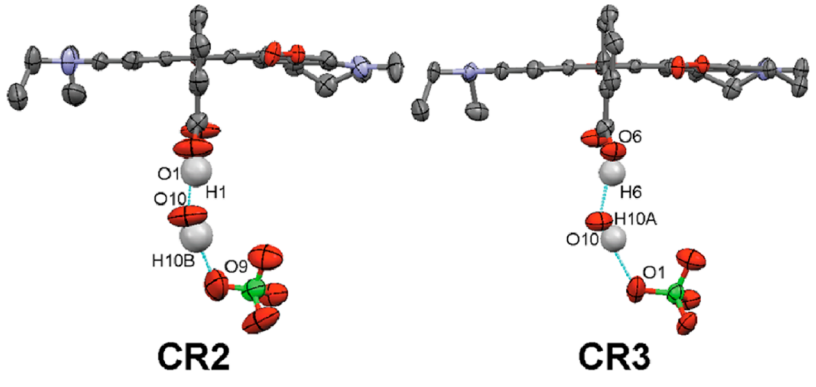

Figure 1. Intermolecular hydrogen bonds (IHB) of compounds **CR2** and **CR3** with ellipsoids shown at the 50% probability level (other hydrogen atoms are omitted for clarity).

the distances of $H_1\cdots O_{10}$ and $H_{10b}\cdots O_9$ for **CR2** were 1.78 and 2.086 Å, respectively.

The representative C−N bond lengths are listed in Table 2 (for atomic labels, see Figure 2). The X-ray crystallographic data showed that the representative C−N bond length *r* values of **CR2** (1.348 and 1.351 Å), **CR3** (1.348 and 1.353 Å), and **CR2E** (1.352 and 1.346 Å) were almost equal. Therefore, π−conjugate interactions existed between the two C−N bonds. The large discrepancy for **CR3E** (1.342 Å and 1.371 Å) may have been caused by intermolecular interactions of its crystalline state.

dx.doi.org/10.1021/jo400783x | J. Org. Chem. 2013, 78, 6121−6130

Table 1. IHB Data of Compounds CR2 and CR3

	$O_a-H_a\cdots O_b$	O_a-H_a (Å)	$H_a\cdots O_b$ (Å)	O_a-O_b (Å)	$O_a-H_a\cdots O_b$ (deg)
CR2	$O_1-H_1\cdots O_{10}$	0.841	1.780	2.586	159.97
	$O_{10}-H_{10b}\cdots O_9$	0.840	2.086	2.926	178.62
CR3	$O_6-H_6\cdots O_{10}$	0.840	1.815	2.618	159.35
	$O_{10}-H_{10a}\cdots O_1$	0.841	2.073	2.892	164.69

Table 2. Crystallographic Data and Theoretical Calculation of Compounds CR2, CR3, CR2E, CR3E, and CR1S

	r^a/r^b (Å)		θ^a/θ^b (deg)
CR2	1.348/1.353	1.351/1.356	88.31/82.69
	N_1-C_7	N_2-C_{30}	$C_{19}-C_{11}-C_{12}-C_{18}$
CR3	1.348/1.353	1.353/1.357	85.34/83.05
	N_1-C_7	N_2-C_{33}	$C_{19}-C_{11}-C_{12}-C_{17}$
CR2E	1.352/1.356	1.346/1.358	98.20/105.14
	N_1-C_{16}	N_2-C_{27}	$C_{11}-C_{12}-C_9-C_8$
CR3E	1.342/1.357	1.371/1.359	104.65/90.41
	N_1-C_{14}	N_2-C_{27}	$C_{22}-C_{20}-C_9-C_8$
CR1S	1.374/1.396 N_1-C_{24}	1.369/1.388 N_2-C_{13}	

[a]The bond data determined from crystal structure. [b]The bond data determined from theoretical calculations.

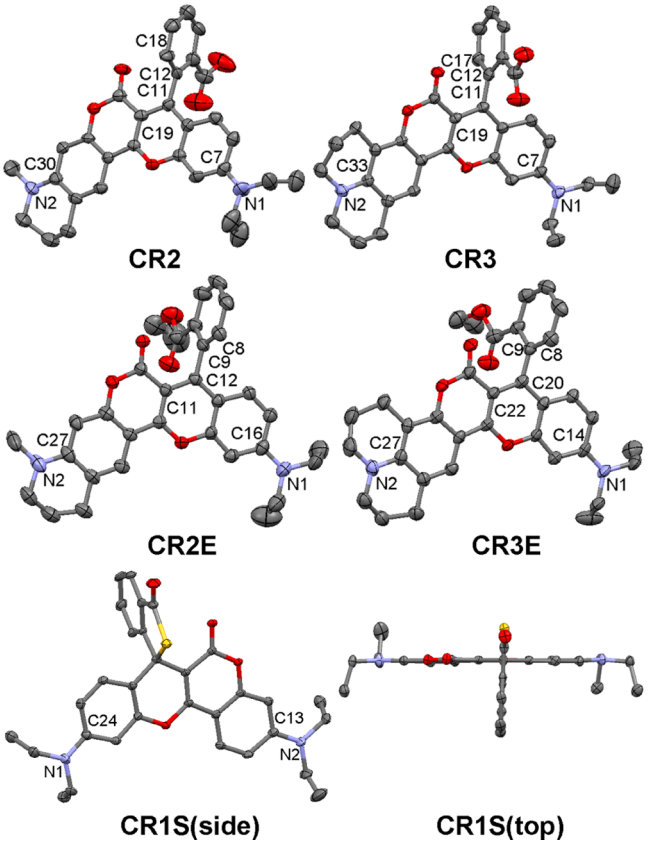

Figure 2. Crystal structures of compounds **CR2**, **CR3**, **CR2E**, **CR3E**, and **CR1S** with ellipsoids shown at the 50% probability level (hydrogen atoms are omitted for clarity).

These conclusions were consistent with the results of density functional theory (DFT) calculations (error ≤0.015 Å; see Table 2). All benzoyl moieties were nearly vertical to the tetracyclic molecular skeletons by their rotation around the bridged single bond. The torsion angles θ of **CR2**, **CR3**, **CR2E**, and **CR3E** are listed in Table 2 (for atomic labels, see Figure 2). The θ values of **CR2** and **CR3** were closer to a vertical angle than those of **CR2E** and **CR3E** because of the small steric hindrance of benzoyl moieties, which were further confirmed by DFT calculations except for **CR3E**. The C−N bond of **CR1S** (1.374 and 1.369 Å) was a single bond, which was longer than that of **CR2** and **CR3**. The benzo[*c*]thiophen-1(3*H*)-one moiety was nearly vertical to the tetracyclic molecular skeleton as shown in Figure 2.

Theoretical Basis. To investigate the geometric and electronic properties of novel deep red dyes, quantum calculations using the Gaussian 03 program[16] were performed. The calculated typical C−N bond lengths and torsion angles are summarized in Table 2. As expected, the results of geometry optimizations were consistent with the experimental data from single crystal structures. The calculated data for **CR3** (1.353 Å, 1.357 Å, and 83.05°) agreed with the experimental data (1.348 Å, 1.353 Å, and 85.34°). Conversely, the calculated data for **CR3E** (1.357 Å, 1.359 Å, and 90.41°) slightly deviated from the corresponding experimental data (1.342 Å, 1.371 Å, and 104.65°). The discrepancy between calculation results and experimental data may have been caused by intermolecular interactions in the actual experiments, such as $\pi-\pi$ stacking or the interaction with counterion. The calculated HOMOs and LUMOs of compounds **CR1** to **CR3** and **CR1E** to **CR3E** are shown in Figure 3. The electron density of these dyes in terms of

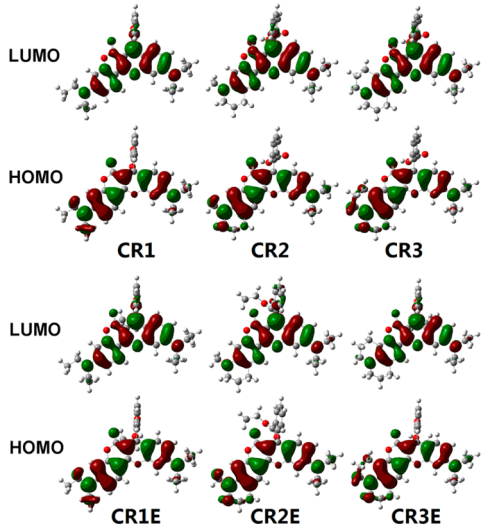

Figure 3. Spatial distributions of calculated HOMOs and LUMOs of compounds **CR1** to **CR3** and **CR1E** to **CR3E**.

the HOMOs and LUMOs was predominantly localized in the tetracyclic structures. These dyes exhibited ICT characteristics of the coumarin moiety. The benzoyl moieties had little influence on photophysical properties because only a small portion of the electron density was localized in their structures. This result was further confirmed by the photophysical properties of the dyes.

Photophysics. To study the structure−property relationships, we investigated the photophysical properties of **CR1** to **CR3** and **CR1E** to **CR3E**. Compounds **CR1** to **CR3** were sensitive to environmental pH because of the −COOH group at the 2′-position. We first examined the absorption profiles of **CR1** to **CR3** and **CR1E** to **CR3E** at different pH levels (Figure 4). The absorption of **CR1** to **CR3** significantly decreased within the pH range from 2 to 4, whereas their absorption was stable at pH > 4

dx.doi.org/10.1021/jo400783x | *J. Org. Chem.* 2013, 78, 6121−6130

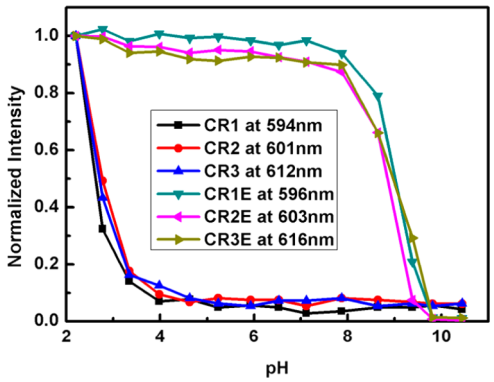

Figure 4. pH dependence of the absorption intensity of compounds **CR1** to **CR3** and **CR1E** to **CR3E** (c = 5 μM).

because of the occurrence of their spirocyclic forms. Consequently, the spirocyclic and open-ring forms of **CR1** to **CR3** were in equilibrium, which was similar to the properties of other rhodamine derivatives. To ensure the formation of open-ring forms, the photophysics of **CR1** to **CR3** was investigated in different solvents with 0.5% trifluoroacetic acid. The absorption of **CR1E** to **CR3E** was independent of the solution pH (from 2 to 8) because these compounds lack the unique spirocyclic/open-ring process of rhodamines. However, the absorption of **CR1E** to **CR3E** was remarkably decreased at the pH range of 8 to 10 because of the open ring of coumarin moieties in basic solutions. Thus, compounds **CR1E** to **CR3E** were suitable deep red fluorescence imaging reagents under the physiological condition.

The absorption and fluorescence spectra of **CR1** to **CR3** and **CR1E** to **CR3E** were investigated in $CHCl_3$, C_2H_5OH, and H_2O (Figure 5, Figures S1 and S2, Supporting Information,

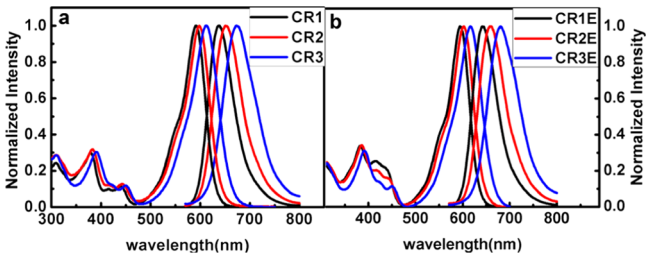

Figure 5. Absorption and fluorescence spectra of (a) compounds **CR1** to **CR3** in C_2H_5OH with 0.5% trifluoroacetic acid and (b) compounds **CR1E** to **CR3E** in C_2H_5OH (c = 5 μM).

respectively). The corresponding photophysical data is summarized in Table 3. The absorption and fluorescence peaks in C_2H_5OH were red-shifted in both the **CR1** → **CR2** → **CR3** and **CR1E** → **CR2E** → **CR3E** series, with the increasing donor property of the amino group in the coumarin moiety. Similar results were obtained in $CHCl_3$ and H_2O because of the increased ICT characteristics of the coumarin moiety. Compounds **CR1** to **CR3** and **CR1E** to **CR3E** showed a larger Stokes shift than the classic rhodamine dyes (Figure 5). For example, **CR3E** exhibited a Stokes shift about 1549 cm^{-1} (65 nm) in C_2H_5OH, which was more than twice that of Rhodamine B (600 cm^{-1}, 19 nm).[7a] The molar extinction coefficients of **CR1** to **CR3** in $CHCl_3$ and C_2H_5OH were ~70000 M^{-1} cm^{-1}, whereas those of **CR1E** to **CR3E** in $CHCl_3$, C_2H_5OH, and H_2O ranged from ~64000 M^{-1} cm^{-1} to ~108000 M^{-1} cm^{-1}. The fluorescence quantum yields of **CR1** and **CR1E** in $CHCl_3$ were 0.507 and 0.494, respectively, which are significant for deep red fluorescent dyes. However, the fluorescence quantum yields of **CR1E** to **CR3E** in H_2O only ranged from 0.002 to 0.014. Thus, biological imaging using **CR1E** to **CR3E** could provide strong contrast, and almost no background fluorescence would be observed. The fluorescence quantum yields decreased in both the **CR1** → **CR2** → **CR3** and **CR1E** → **CR2E** → **CR3E** series as the energy gap was decreased.[17] This result is consistent with the literature.[7a,18] The −COOH and $-COOC_2H_5$ groups had little influence on the photophysical properties, as compared with **CR1** and **CR1E** in different solvents. These results were previously predicted by the DFT calculations.

Intracellular Imaging for Mitochondria (CR1E to CR3E). The molecular structures of **CR1E** to **CR3E** contain a positive charge and are highly similar to those of the mitochondria-specific fluorescent dyes MTR and Rhodamine 123.[3] Thus, these positively charged deep red dyes may preferentially accumulate in mitochondria by electrostatic interactions. The electrostatic interactions can accumulate and increase by a 100-fold to 500-fold, as described by the Nernst equation.[13a] To demonstrate this possibility, novel deep red fluorescent dyes **CR1E** to **CR3E** were incubated with living A549 cells (Figure 6). The localization of dyes' accumulation could be confirmed by dual-channel laser scanning confocal microscopy in the costaining experiments. The extensive overlapping with MitoTracker Green FM (MTG) indicated that these deep red dyes were able to efficiently penetrate the cell membrane and specifically label mitochondria. These results revealed the potential imaging and therapeutic applications of these novel deep red dyes. To confirm their mechanism of accumulation in mitochondria, carbonyl cyanide 3-chlorophenylhydrazone (CCCP) was used to change MMP before the staining procedure. Upon treatment with CCCP, the MMP was lost because of the rapid acidification of mitochondria and the dysfunction of ATP synthase.[20] After treatment with 30 μM CCCP, fluorescence intensity in mitochondria became faint, because the decreasing MMP affected the accumulation of the cationic dye (**CR1E** to **CR3E**) in mitochondria (Figure S3, Supporting Information).

As is well-known, photostability is very important for fluorescent dyes due to the temporal monitoring of dynamic events inside cells. To evaluate the practical utility of the novel deep red dyes, their photostability in PBS buffer was performed by continuous irradiation of compounds **CR1E** to **CR3E** (compared with MitoTrackers) using a 500 W Xe lamp as the light source. After 30 min continuous irradiation, the absorption intensity of **CR1E** to **CR3E** decreased to 76% to 84%, whereas that of MTR dropped to 64% as shown in Figure 7. It is significant that the photostability of **CR1E** to **CR3E** was much higher than that of cyanine dyes, such as MTG (7%) and MitoTracker Deep Red FM (MTDR, 12%). The cytotoxicity of **CR1E** to **CR3E** in A549 cells was examined using the MTT (3-(4,5-dimethylthiazol-2-yl)-2,5-diphenyl-2*H*-tetrazolium bromide) assay. The cytotoxicities of MTG, MTR, and MTDR were tested as the controls. Compounds **CR1E** to **CR3E** exhibited low cytotoxicity (cell viability >90%) at concentrations up to 100 nM after incubation with A549 cells for 24 h (Figure 8). However, MTG and MTDR reduced the cell viability below 90% even at 10 nM.

These deep red emissive properties helped reduce the interference of autofluorescence from biomolecules in the organism and obtained a higher signal-to-noise ratio. To evaluate the potential imaging and diagnostic applications of novel deep

dx.doi.org/10.1021/jo400783x | J. Org. Chem. 2013, 78, 6121−6130

Table 3. Photophysical Properties of Compounds CR1 to CR3 and CR1E to CR3E

compd	solvent	λ_{max} (nm)	λ_{em} (nm)	Stokes shift (nm/cm^{-1})	ε^b (M^{-1}cm^{-1})	Φ^c	τ (ns)
CR1[a]	$CHCl_3$	602	636	34/888	77400	0.51	4.16
	C_2H_5OH	591	637	46/1222	70800	0.21	2.29
	H_2O	594	646	52/1355	26800	0.01	0.31
CR2[a]	$CHCl_3$	610	647	37/937	76600	0.27	3.79
	C_2H_5OH	598	651	53/1361	64800	0.05	0.98
	H_2O	601	658	57/1441	44800	<0.01	0.15
CR3[a]	$CHCl_3$	623	664	41/991	75000	0.09	2.87
	C_2H_5OH	612	674	62/1503	69200	0.01	0.47
	H_2O	612	684	72/1720	38600	<0.01	0.16
CR1E	$CHCl_3$	601	640	39/1014	99000	0.49	4.31
	C_2H_5OH	595	642	47/1230	64000	0.20	2.12
	H_2O	596	652	56/1441	71600	0.01	0.27
CR2E	$CHCl_3$	608	647	39/991	108000	0.33	4.07
	C_2H_5OH	602	658	56/1414	77800	0.04	0.86
	H_2O	602	666	64/1596	76200	<0.01	0.16
CR3E	$CHCl_3$	625	669	44/1052	107800	0.11	3.44
	C_2H_5OH	616	681	65/1549	87600	0.01	0.43
	H_2O	616	687	71/1678	66200	<0.01	0.13

[a]The photophysics are investigated in different solvents with 0.5% trifluoroacetic acid. [b]The molar extinction coefficients at maximum absorption. [c]Using cresyl violet in methanol as the reference (Φ = 0.54).[19]

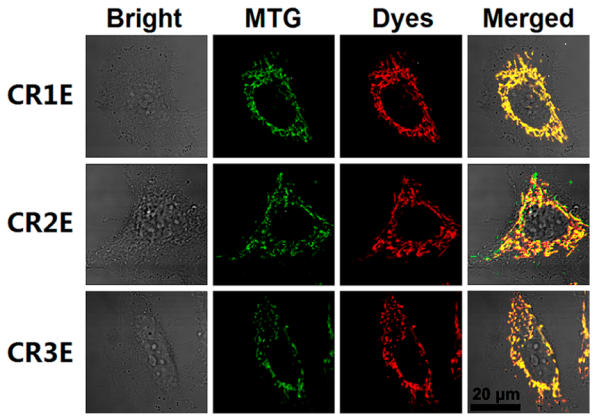

Figure 6. Confocal fluorescence microscopy images of A549 incubated with MTG (10 nM) and compounds **CR1E** to **CR3E** (50 nM).

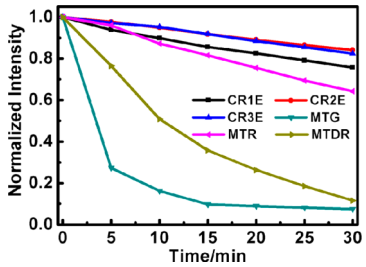

Figure 7. Photostability of compounds **CR1E** to **CR3E** and MitoTrackers (5 μM) in PBS buffer (pH = 7.4).

red dyes, **CR1E** to **CR3E** were incubated with different cell lines (cancer cells, A549 and HeLa; normal cells, L929). As shown in Figures S4–S6 (Supporting Information), the strong intracellular fluorescence may be attributed to the distribution of dyes in the inner mitochondrial membrane, where a relatively organic-like mitochondrial matrix of cancer and normal cells exists. Although the fluorescence quantum yields of **CR1E** to **CR3E** were relatively low (0.002–0.014) in a polar solvent (H_2O), the fluorescence intensity in mitochondria was sufficient to provide

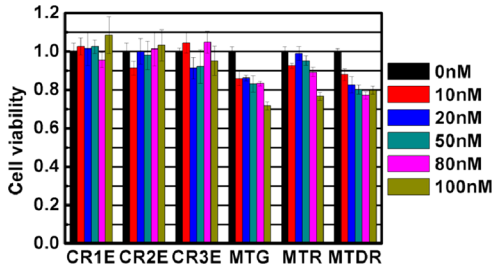

Figure 8. Cytotoxicity of compounds **CR1E** to **CR3E** and MitoTrackers in A549 cells.

strong contrast for imaging due to its enrichment inside mitochondria. The morphologies of mitochondria in cancer and normal cells can be clearly visualized. Furthermore, almost no background fluorescence could be observed, especially in the nucleus. To demonstrate the compatibility of **CR1E** to **CR3E** with other dyes such as Hoechst 33342, costaining experiments were performed. We were able to clearly visualize the blue nuclear staining in the DAPI channel and the red mitochondrial staining by the novel dyes in the Cy5 channel (Figure 9). The superimposition patterns between **CR1E** to **CR3E** and Hoechst 33342 allowed for the simultaneous imaging of mitochondria and DNA.

Ratiometric Bioimaging for Hg^{2+} (CR1S). Based on the well-known desulfurization reaction, we developed a new ratiometric sensor (**CR1S**, Scheme 1) for Hg^{2+} in this work. With compound **CR1S** in hand, we first investigated its absorption response to Hg^{2+} at different pH levels (Figure S7, Supporting Information). The intensities of compound **CR1S** solutions in a citric acid (0.1 M)–phosphate (0.2 M) buffer (H_2O/CH_3OH = 1:1, v/v) within pH 2 to 8 were found to be stable. However, the addition of Hg^{2+} resulted in a distinct increasing in the absorption intensity at 596 nm with increasing acidity (from pH 8 to 2), which was similar with the reported Hg^{2+} sensor.[15] According to reference, we chose pH = 4 as the measuring conditions.

Figure 10 showed the spectroscopic properties of **CR1S** at various Hg^{2+} concentrations in a citric acid (0.1 M)–phosphate

dx.doi.org/10.1021/jo400783x | J. Org. Chem. 2013, 78, 6121–6130

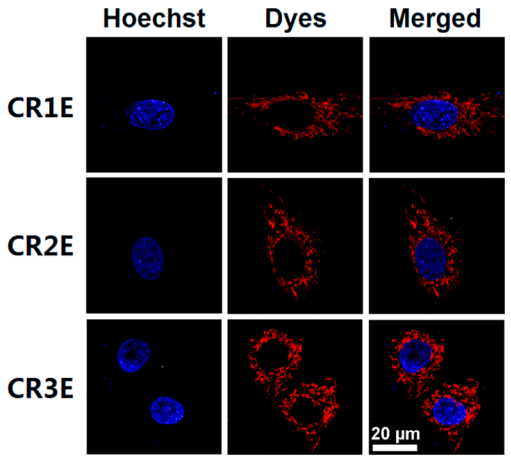

Figure 9. Confocal fluorescence microscopy images of A549 cells incubated with Hoechst 33342 (1 mg/mL) and compounds **CR1E** to **CR3E** (50 nM).

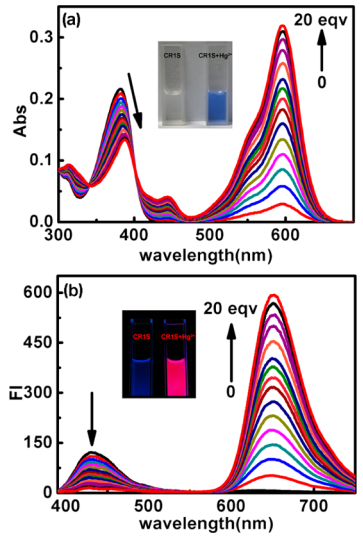

Figure 10. Absorption (a) and fluorescence spectra (b) of **CR1S** (5 μM) with different Hg^{2+} concentrations in a citric acid (0.1 M)−phosphate (0.2 M) buffer (pH = 4, H_2O/CH_3OH = 1:1, v/v). λ_{ex} = 380 nm. The insets show the color changes and fluorescence changes in the absence and presence of Hg^{2+}.

(0.2 M) buffer (pH = 4, H_2O/CH_3OH = 1:1, v/v). The UV/vis spectra of **CR1S** only showed the absorption profile from the coumarin moiety of the spirocyclic form with a maximum at 381 nm (Figure 10a). The addition of Hg^{2+} immediately decreased the absorption peak at 381 nm with red-shifted and a new absorption band at 596 nm appeared, which corresponded to the absorption of rhodamine-like moiety. The spectral shifts were about 215 nm, and two isosbestic points at 340 and 400 nm were formed. They exhibited a clear color change from colorless to blue, and colorimetric performance could be easily monitored by the naked eye for instantaneous visual sensing (inset, Figure 10a). Similar ratio changes can also be observed from the fluorescence spectra (Figure 10b). The intensity at 430 nm from the coumarin moiety decreased and that at 653 nm from rhodamine-like moiety gradually increased with increasing Hg^{2+} concentration. Indeed, this coumarin- and rhodamine-fused π-conjugated system had very large spectral shifts of up to 223 nm, which were much larger than those of TBET or FRET-based rhodamine systems.[21] In addition, such fluorescence performance could be detected by the naked eye as depicted in the inset of Figure 10b, where photos of solutions of compound **CR1S** before and after addition of Hg^{2+} under UV light irradiation were displayed.

As shown in Figure S8 (Supporting Information), the linear fitting can be obtained between Hg^{2+} concentrations ranging from 0 to 100 μM and the absorption ratio (A_{596}/A_{381}) as well as the square root of fluorescence intensity ratio ($I^{1/2}_{653}/I^{1/2}_{430}$) of **CR1S**, respectively. The response to Hg^{2+} of **CR1S** was also very fast, and spectral data were recorded within 10 s after the addition of Hg^{2+}. The selectivity of **CR1S** for different metal ions was also investigated. As shown in Figure S9 (Supporting Information), the fluorescence response of **CR1S** displayed excellent selectivity to Hg^{2+} over all other tested ions. We proposed that the high thiophilicity of Hg^{2+} resulted in the formation of the open-ring complex, and then hydrolyzed to **CR1**. This result can be confirmed by the ESI-MS signals at m/z 511.2 (corresponding to **CR1**) in the solution of **CR1S** treated with excess Hg^{2+} (Figure S10, Supporting Information).

Taking into account of the advantages of ratiometric fluorescence changes, compound **CR1S** was used for in vitro Hg^{2+} detection in living A549 cells. As shown in Figure 11a, A549 cells incubated with **CR1S** (2 μM) for 10 min showed a clear blue fluorescence, whereas weak red fluorescence was observed in the red channel, which indicated that **CR1S** mainly existed in the spirolactam form. After Hg^{2+} (20 μm) treatment for 10 min, the blue fluorescence intensity decreased and the red fluorescence intensity significantly increased (Figure 11b). As shown in the ratio imaging (Red/Blue) in Figure 11, distinct changes in ratio fluorescence responses in A549 cells were observed. This indicated the potential of biological imaging application of the new ratiometric deep red sensor.

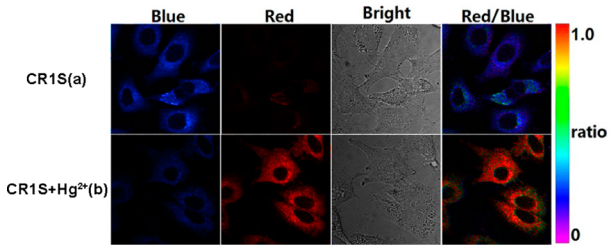

Figure 11. Confocal fluorescence imaging of Hg^{2+} in A549 cells with (a) **CR1S** (2 μm) for 10 min and (b) **CR1S** (2 μm) for 10 min and then Hg^{2+} (20 μm) for 10 min.

CONCLUSIONS

We have introduced a new strategy to design deep red fluorescent dyes (**CR1** to **CR3**) containing a coumarin- and rhodamine-fused conjugated skeleton. The novel deep red fluorescent dyes have excellent photophysical properties, such as high molar extinction coefficients, excellent fluorescence quantum yields in $CHCl_3$, great photostability, and a large Stokes shift. Importantly, these dyes **CR1** to **CR3** could undergo equilibrium between the coumarin moiety and rhodamine-like fluorophore switched by the spirocyclic/open-ring process of the −COOH, which can be used as versatile sensing platform for designing ratiometric fluorescent sensors. Considering their good photophysical properties, we designed a series of deep red fluorescent bioimaging agents (**CR1E** to **CR3E**) by esterification of **CR1** to **CR3**, which can selectively stain mitochondria. Cell-imaging experiments indicated that these dyes were superior over

dx.doi.org/10.1021/jo400783x | J. Org. Chem. 2013, 78, 6121−6130

MitoTrackers because of their deep red emission with large Stokes shift, excellent contrast for imaging, high photostability, and low cytotoxicity. Furthermore, using **CR1** as a platform, we developed a novel ratiometric sensor (**CR1S**) for mercury ions with the decreased fluorescence of coumarin moiety and large turn-on deep red fluorescence of rhodamine-like moiety. **CR1S** could be successfully applied to the ratiometric imaging of Hg^{2+} in living A549 cells. This design strategy may be extended for development of new deep red fluorescent dyes by simply introducing different fluorophores, and dyes **CR1** to **CR3** will be good candidates for biosensors, biomarkers, and bioimaging.

EXPERIMENTAL SECTION

Materials and Methods. All commercial chemicals were used without further purification. Compound **2** (7-amino-1-methyl-1,2,3,4-tetrahydroquinoline hydrochloride) was purchased from HangZhou Trylead Chemical Technology Co., Ltd. MTG, MTR, MTDR, and Hoechst were purchased from Invitrogen (USA). CCCP was purchased from Alfa Aesar. Crystallographic data of **CR2**, **CR3** and **CR2E** were done on a Saturn724+ CCD with Mo Kα radiation (λ = 0.71073 Å) at 173 K. Crystallographic data of **CR3E** was done on a Rigaku raxis rapid IP area detector with Cu Kα radiation (λ = 1.54178 Å) at 173 K. Crystallographic data of **CR1S** were obtained on an image plate X-ray diffractameter with Mo Kα radiation (λ = 0.71073 Å) at 293 K. The quantum chemical calculations were optimized using the restricted B3LYP functions with a 6-31G(d) basis set at the DFT level. ^{1}H NMR and ^{13}C NMR spectra were recorded at 400 and 100 MHz respectively. The HRMS were measured with Fourier transform ion cyclotron resonance mass spectrometry (FTICR-MS). Absorption and fluorescence spectra of all compounds were obtained in an absorption spectrometer and a fluorescence spectrometer at room temperature, respectively. The fluorescence lifetimes were measured in a FLS920 combined steady-state and time-resolved fluorescence spectrometer. A549, HeLa, and L929 cells (gifted from the center of cells, Peking Union Medical College) were cultured in confocal dishes in culture media (McCoy's 5A, DMEM or RPM1640 respectively, supplemented with 10% FBS, 50 unit/mL penicillin, and 50 mg/mL of streptomycin) under 5% carbon dioxide/air at 37 °C in a humidified incubator for 24 h. The cells were washed with PBS three times before fluorescent imaging. Confocal microscopy and image analysis was acquired with a laser scanning confocal microscopy (for Hoechst 33342, excited at 405 nm, DAPI channel; for MTG, excited at 488 nm, FITC channel; for **CR1E** to **CR3E**, excited at 640 nm, Cy5 channel). The microscope was equipped with a live-cell incubation chamber maintaining a humidified atmosphere of 37 °C and 5% CO_2. Images were processed by NIS-Elements Viewer 3.20.

Synthesis of 7-Diethylamino-4-hydroxycoumarin (4). 3-Diethylaminophenol **1** (12.8 g, 77.5 mmol) and diphenyl malonate **8** (18.8 g, 73.4 mmol) were added into anhydrous toluene (50 mL). The mixture was heated to reflux for 4 h, and compound **4** was obtained by filtration as gray solid (5.2 g, 30%):[22] mp 233−235 °C; ^{1}H NMR (400 MHz, DMSO) δ (ppm) 11.98 (s, 1H), 7.55−7.53 (d, 1H, J = 9.0 Hz), 6.67−6.64 (dd, 1H, J_1 = 2.2 Hz, J_2 = 9.0 Hz), 6.45−6.44 (d, 1H, J = 2.2 Hz), 5.23 (s, 1H), 3.43−3.38 (q, 4H, J = 7.0 Hz), 1.13−1.09 (t, 6H, J = 7.0 Hz); ^{13}C NMR (100 MHz, DMSO) δ (ppm) 166.7, 162.8, 156.1, 150.8, 124.1, 108.1, 103.6, 96.4, 86.1, 44.0, 12.3; ESI-HRMS m/z calcd for $[C_{13}H_{15}NO_3+H]^+$ 234.11247, found 234.11205.

Synthesis of 7-Hydroxy-1-methyl-1,2,3,4-tetrahydroquinolin (5). Compound **2** (3.2 g, 1.6 mmol) was added into 85% phosphoric acid (15 mL) and heated to reflux for 24 h.[23] After being cooled to room temperature, the reaction solution was neutralized with 200 mL of 40% NaOH aqueous solution. A large amount of Na_3PO_4 was precipitated and filtrated. The filtrate was extracted with CH_2Cl_2 (total 60 mL for three times). The organic phase was concentrated under vacuum and purified by column chromatography to afford compound **5** as white solid using v($CH_3COOC_2H_5$)/v(petroleum ether) = 1:3 as the eluent (1.3g, 48%): mp 103−104 °C; ^{1}H NMR (400 MHz, DMSO) δ (ppm) 8.74 (s, 1H), 6.64−6.62 (d, 1H, J = 7.9 Hz), 5.98−5.97 (d, 1H, J = 2.1 Hz), 5.95−5.93 (dd, 1H, J_1 = 2.2 Hz, J_2 = 7.9 Hz), 3.13−3.10 (t, 2H, J = 5.6 Hz), 2.75 (s, 3H), 2.57−2.54 (t, 2H, J = 6.4 Hz), 1.86−1.80 (m, 2H); ^{13}C NMR (100 MHz, DMSO) δ (ppm) 156.4, 147.3, 128.9, 112.9, 102.9, 98.2, 50.5, 38.7, 26.5, 22.3; ESI-HRMS m/z calcd for $[C_{10}H_{13}NO + H]^+$ 164.10699, found 164.10657.

Synthesis of 4-Hydroxy-9-methyl-6,7,8,9-tetrahydropyrano-[3,2-*g*]quinolin-2-one (6). Compound **5** (1.0 g, 3.9 mmol) and diphenyl malonate **8** (0.64 g, 3.9 mmol) were added into anhydrous toluene (8 mL). The mixture was heated to reflux for 6 h, and compound **6** was obtained by filtration as gray solid (0.8 g, 88%):[22] mp 255−257 °C; ^{1}H NMR (400 MHz, DMSO) δ (ppm) 11.83 (s, 1H), 7.26 (s, 1H), 6.35 (s, 1H), 5.23 (s, 1H), 3.33−3.31 (t, 2H, J = 5.6 Hz), 2.92 (s, 3H), 2.73−2.70 (t, 2H, J = 6.1 Hz), 1.87−1.84 (t, 2H); ^{13}C NMR (100 MHz, DMSO) δ (ppm) 166.4, 162.7, 154.7, 149.7, 121.7, 118.8, 103.2, 95.5, 86.0, 50.0, 38.5, 26.6, 21.2; ESI-HRMS m/z calcd for $[C_{13}H_{13}NO_3 + H]^+$ 232.09682, found 232.09648.

Synthesis of 4-Hydroxypyrano[3,2-*g*]julolidine-2-one (7). 8-Hydroxyjulolidine **3** (3.7 g, 19.3 mmol) and diphenyl malonate **8** (4.1 g, 15.9 mmol) were added into anhydrous toluene (10 mL). The mixture was heated to reflux for 4 h, and compound **7** was obtained by filtration as a straw yellow solid (3.6 g, 88%):[22] mp 268−270 °C; ^{1}H NMR (400 MHz, DMSO) δ (ppm) 11.73 (s, 1H), 7.15 (s, 1H), 5.21 (s, 1H), 3.24−3.20 (m, 4H), 2.70 (s, 4H), 1.91−1.83 (m, 4H); ^{13}C NMR (100 MHz, DMSO) δ (ppm) 166.5, 162.8, 151.0, 146.0, 119.8, 117.3, 105.3, 103.1, 85.8, 49.2, 48.7, 26.9, 21.0, 20.1, 20.0; ESI-HRMS m/z calcd for $[C_{15}H_{15}NO_3 + H]^+$ 258.11247, found 258.11210.

Synthesis of Compound CR1. Compound **4** (440 mg, 1.9 mmol) and 2-(4-diethylamino-2-hydroxy)-benzoylbenzoic acid **9** (629 mg, 2.0 mmol) were heated to reflux in 15 mL of 1,1,2,2-tetrachloroethane until the substances have dissolved completely. A total of 2.8 g phosphorus pentoxide was then added in portions, and the reaction mixture was heated to reflux for 4 h.[24] After cooling, the mixture was dissolved using water (25 mL) and chloroform (25 mL), and the water phase was extracted with chloroform (total 100 mL for three times). The combined organic phases were concentrated under vacuum and purified by column chromatography using v(CH_2Cl_2)/v(CH_3OH) = 100:1 as the eluent. The dye fractions were concentrated under vacuum, and the residue was dissolved in 2 mL ethanol. After addition of 3 mL perchloric acid (note: the operation should be executed very carefully due to the instability of perchlorate salts), the solution was precipitated by dropwise addition of water (100 mL). Compound **CR1** was obtained by filtration as a dark green solid (682 mg, 59%): mp 287−289 °C; ^{1}H NMR (400 MHz, DMSO) δ (ppm) 8.02−7.94 (m, 2H), 7.71−7.60 (m, 2H), 7.31−7.29 (d, 1H), 6.90−6.87 (m, 2H), 6.68 (s, 1H), 6.60−6.55 (m, 2H), 3.52−3.44 (m, 8H), 1.16−1.11 (m, 12H); ^{13}C NMR (100 MHz, CD_3OD/CD_2Cl_2) δ (ppm) 166.9, 163.6, 163.4, 158.7, 158.4, 158.0, 157.9, 156.6, 136.8, 133.7, 132.9, 131.4, 130.4, 129.6, 128.8, 127.8, 116.9, 116.7, 112.7, 104.6, 101.3, 98.0, 97.9, 52.9, 47.2, 46.4, 12.7; ESI-HRMS m/z calcd for $[C_{31}H_{31}N_2O_5]^+$ 511.22275, found 511.22229. Anal. Calcd for $C_{31}H_{31}ClN_2O_9 \cdot {}^1/_2H_2O$: C, 60.05; H, 5.20; N, 4.52. Found: C, 60.11; H, 5.14; N, 4.33.

Synthesis of Compound CR2. Compound **6** (659 mg, 2.9 mmol) and 2-(4-diethylamino-2-hydroxy)benzoylbenzoic acid **9** (1.1 g, 3.5 mmol) were heated to reflux in 20 mL of 1,1,2,2-tetrachloroethane until the substances have dissolved completely. A total of 4.0 g of phosphorus pentoxide was then added in portions, and the reaction mixture was heated to reflux for 4 h.[24] After cooling, the mixture was dissolved using water (25 mL) and chloroform (25 mL), and the water phase was extracted with chloroform (total 100 mL for three times). The combined organic phases were concentrated under vacuum and purified by column chromatography using v(CH_2Cl_2)/v(CH_3OH) = 100:1 as the eluent. The dye fractions were concentrated under vacuum, and the residue was dissolved in 3 mL ethanol. After addition of 5 mL perchloric acid (note: the operation should be executed very carefully due to the instability of perchlorate salts), the solution was precipitated by dropwise addition of water (100 mL). Compound **CR2** was obtained by filtration as dark green solid (720 mg, 42%): mp 289−290 °C; ^{1}H NMR (400 MHz, DMSO) δ (ppm) 7.97−7.96 (m, 1H), 7.74−7.60 (m, 3H), 7.29−7.27 (m, 1H), 6.87 (s, 1H), 6.69 (s, 1H), 6.57 (s, 1H), 6.49 (s, 1H), 3.44 (s, 6H), 3.01 (s, 3H), 2.84−2.81 (t, 2H, J = 5.8 Hz), 1.92 (s,

dx.doi.org/10.1021/jo400783x | J. Org. Chem. 2013, 78, 6121−6130

2H), 1.15−1.12 (t, 6H, J = 6.8 Hz); ^{13}C NMR (100 MHz, CD_3OD/CD_2Cl_2) δ (ppm) 168.2, 162.9, 158.2, 157.9, 157.5, 155.7, 137.5, 133.5, 132.8, 131.7, 130.4, 130.3, 128.5, 124.3, 124.2, 116.4, 104.4, 101.2, 98.0, 96.7, 52.4, 47.2, 40.0, 27.8, 21.8, 12.8; ESI-HRMS m/z calcd for $[C_{31}H_{29}N_2O_5]^+$ 509.20710, found 509.20627. Anal. Calcd for $C_{31}H_{29}ClN_2O_9 \cdot {}^3/_2H_2O$: C, 58.54; H, 5.07; N, 4.40. Found: C, 58.33; H, 4.80; N, 4.49.

Synthesis of Compound CR3. Compound **7** (1.2 g, 4.7 mmol) and 2-(4-diethylamino-2-hydroxy)benzoylbenzoic acid **9** (1.8 g, 5.7 mmol) were heated to reflux in 50 mL of 1,1,2,2-tetrachloroethane until the substances have dissolved completely. A total of 7.8 g of phosphorus pentoxide was then added in portions, and the reaction mixture was heated to reflux for 4 h.[24] After cooling, the mixture was dissolved using water (25 mL) and chloroform (25 mL), and the water phase was extracted with chloroform (total 100 mL for three times). The combined organic phases were concentrated under vacuum and purified by column chromatography using v(CH_2Cl_2)/v(CH_3OH) = 100:1 as the eluent. The dye fractions were concentrated under vacuum, and the residue was dissolved in 5 mL of ethanol. After addition of 10 mL of perchloric acid (note: the operation should be executed very carefully due to the instability of perchlorate salts), the solution was precipitated by dropwise addition of water (150 mL). Compound **CR3** was obtained by filtration as dark green solid (982 mg, 33%): mp 290−292 °C; ^{1}H NMR (400 MHz, DMSO) δ (ppm) 8.04−8.03 (m, 1H), 7.74−7.62 (m, 3H), 7.28−7.26 (m, 1H), 6.92−6.64 (m, 3H), 3.49−3.36 (m, 8H), 2.81−2.78 (m, 2H), 2.65−2.64 (m, 2H), 1.94−1.83 (m, 4H), 1.16−1.13 (t, 6H, J = 6.9 Hz); ^{13}C NMR (100 MHz, CD_3OD/CD_2Cl_2) δ (ppm) 167.1, 161.8, 157.4, 157.3, 156.5, 152.3, 152.0, 136.3, 132.5, 131.8, 130.9, 129.4, 129.3, 127.6, 122.3, 122.1, 115.2, 115.1, 106.3, 103.5, 100.0, 96.9, 50.8, 50.3, 46.2, 27.2, 20.6, 19.6, 19.5, 11.9; ESI-HRMS m/z calcd for $[C_{33}H_{31}N_2O_5]^+$ 535.22275, found 535.22213. Anal. Calcd for $C_{33}H_{31}ClN_2O_9$: C, 62.41; H, 4.92; N, 4.41. Found: C, 63.28; H, 5.46; N, 4.14.

Synthesis of Compound CR1E. Concentrated H_2SO_4 (0.5 mL) was added to an ethanol solution of compound **CR1** (120 mg, 0.2 mmol), and the solution was heated to reflux for 2 h.[25] After cooling, ethanol was removed under vacuum, and the residue was neutralized with 20 mL of 10% NaOH aqueous solution to collect the resulting precipitate. After drying, it was purified by silica gel chromatography using v(CH_2Cl_2)/v(CH_3OH) = 100:1 as the eluent to give **CR1E** as a dark green solid (39 mg, 31%): mp 272−274 °C; ^{1}H NMR (400 MHz, DMSO) δ (ppm) 8.20−8.17 (m, 2H), 7.83−7.71 (m, 2H), 7.40−7.31 (m, 2H), 7.20−7.07 (m, 2H), 6.90−6.75 (m, 2H), 4.10−4.08 (q, 2H, J = 7.1 Hz), 3.71−3.60 (m, 8H), 1.23−1.18 (m, 12H), 1.07−1.04 (t, 3H, J = 7.1 Hz); ^{13}C NMR (100 MHz, DMSO) δ (ppm) 164.8, 161.8, 161.2, 157.2, 156.9, 156.6, 156.4, 155.1, 135.6, 133.0, 132.9, 131.4, 130.1, 129.5, 128.3, 126.9, 116.7, 115.4, 111.8, 103.6, 99.9, 97.2, 96.9, 61.1, 54.9, 45.8, 45.0, 13.6, 12.4; ESI-HRMS m/z calcd for $[C_{33}H_{35}N_2O_5]^+$ 539.25405, found 539.25309. Anal. Calcd for $C_{33}H_{35}ClN_2O_9 \cdot {}^1/_2H_2O$: C, 61.16; H, 5.60; N, 4.32. Found: C, 61.29; H, 5.61; N, 4.23.

Synthesis of Compound CR2E. Concentrated H_2SO_4 (1 mL) was added to an ethanol solution of compound **CR2** (505 mg, 0.8 mmol), and the solution was heated to reflux for 2 h.[25] After cooling, ethanol was removed under vacuum, and the residue was neutralized with 40 mL 10% NaOH aqueous solution to collect the resulting precipitate. After drying, it was purified by silica gel chromatography using v(CH_2Cl_2)/v(CH_3OH) = 100:1 as the eluent to give **CR2E** as a dark green solid (350 mg, 66%): mp 279−280 °C; ^{1}H NMR (400 MHz, DMSO) δ (ppm) 8.20−8.18 (m, 1H), 7.90−7.71 (m, 3H), 7.33−7.31 (m, 2H), 7.16−7.13 (m, 1H), 6.88−6.84 (m, 1H), 6.64 (s, 1H), 4.12−4.06 (q, 2H, J = 7.0 Hz), 3.69−3.68 (m, 4H), 3.58−3.55 (m, 2H), 3.15 (s, 3H), 2.87−2.84 (t, 2H, J = 5.7 Hz), 1.96−1.94 (m, 2H), 1.23 (s, 6H), 1.07−1.03 (t, 3H, J = 7.1 Hz); ^{13}C NMR (100 MHz, DMSO) δ (ppm) 164.9, 161.3, 161.1, 156.8, 156.5, 156.4, 156.2, 154.3, 135.6, 132.9, 131.3, 130.1, 129.5, 128.4, 128.3, 123.1, 122.9, 116.3, 115.1, 103.5, 99.6, 97.0, 96.0, 61.1, 54.9, 51.0, 45.8, 26.4, 20.5, 13.7, 12.5; ESI-HRMS m/z calcd for $[C_{33}H_{33}N_2O_5]^+$ 537.23840, found 537.23773. Anal. Calcd for $C_{33}H_{33}ClN_2O_9 \cdot {}^1/_2H_2O$: C, 61.35; H, 5.30; N, 4.34. Found: C, 61.46; H, 5.35; N, 4.30.

Synthesis of Compound CR3E. Concentrated H_2SO_4 (1 mL) was added to an ethanol solution of compound **CR3** (430 mg, 0.7 mmol), and the solution was heated to reflux for 2 h.[25] After cooling, ethanol was removed under vacuum and the residue was neutralized with 40 mL of 10% NaOH aqueous solution to collect the resulting precipitate. After drying, it was purified by silica gel chromatography using v(CH_2Cl_2)/v(CH_3OH) = 100:1 as the eluent to give **CR3E** as a dark green solid (308 mg, 68%): mp 273−274 °C; ^{1}H NMR (400 MHz, DMSO) δ (ppm) 8.20−8.18 (m, 1H), 7.83−7.70 (m, 3H), 7.32−7.30 (m, 2H), 7.12−7.10 (m, 1H), 6.84−6.82 (m, 1H), 4.09−4.07 (m, 2H), 3.68−3.66 (m, 4H), 3.51−3.48 (m, 4H), 2.86 (s, 2H), 2.69 (s, 2H), 1.95−1.90 (m, 4H), 1.23 (s, 6H), 1.06−1.03 (t, 3H, J = 7.0 Hz); ^{13}C NMR (100 MHz, DMSO) δ (ppm) 164.8, 161.0, 160.9, 156.8, 156.5, 156.0, 151.6, 151.3, 135.7, 132.8, 131.2, 130.1, 129.4, 128.2, 122.0, 121.6, 115.9, 114.8, 105.7, 103.3, 99.3, 97.0, 61.0, 50.3, 49.7, 45.6, 26.7, 20.3, 19.4, 19.1, 13.6, 12.5; ESI-HRMS m/z calcd for $[C_{35}H_{35}N_2O_5]^+$ 563.25405, found 563.25315. Anal. Calcd for $C_{35}H_{35}ClN_2O_9 \cdot {}^1/_2H_2O$: C, 62.54; H, 5.40; N, 4.17. Found: C, 62.59; H, 5.37; N, 4.15.

Synthesis of Compound CR1S. Compounds **CR1** (150 mg, 0.25 mmol) and phosphorus oxychloride (1 mL) were added into 1,2-dichloromethane (5 mL), and the mixture was heated to reflux for 4 h.[15] After cooling, the reaction mixture was concentrated under vacuum to obtain crude acyl chloride. Saturated Na_2S aqueous solution (5 mL, 1.2 g) was then added to the crude acyl chloride, and the mixture was stirred for 3 h at room temperature. Following extraction with ethyl acetate (total 100 mL for three times), the organic phase was purified by column chromatography using CH_2Cl_2 as the eluent to afford the pale yellow solid **CR1S** in 56% yield (72 mg): mp 301−302 °C; ^{1}H NMR (400 MHz, $CDCl_3$) δ (ppm) 7.88−7.85 (m, 2H), 7.51−7.41 (m, 2H), 7.21−7.19 (m, 1H), 6.72−6.64 (m, 2H), 6.44−6.38 (m, 2H), 3.45−3.33 (m, 8H), 1.23−1.17 (m, 12H); ^{13}C NMR (100 MHz, CDCl3) δ (ppm) 197.4, 159.7, 158.0, 156.8, 155.6, 151.4, 149.8, 148.5, 136.5, 133.8, 130.4, 128.0, 125.4, 124.4, 123.0, 110.2, 108.9, 108.8, 102.0, 97.4, 97.1, 95.8, 58.5, 44.9, 44.5, 12.7, 12.5; ESI-HRMS m/z calcd for $[C_{31}H_{30}N_2O_4S + H]^+$ 527.19990, found 527.20044. Anal. Calcd for $C_{31}H_{30}N_2O_4S \cdot {}^1/_4H_2O$: C, 70.10; H, 5.79; N, 5.27. Found: C, 70.19; H, 5.91; N, 5.19.

■ ASSOCIATED CONTENT

Supporting Information

X-ray structure details of compounds **CR2**, **CR3**, **CR2E**, **CR3E**, and **CR1S** (CIF); photophysical data; imaging data; sensor data and ^{1}H NMR and ^{13}C NMR spectra of new compounds. This material is available free of charge via the Internet at http://pubs.acs.org.

■ AUTHOR INFORMATION

Corresponding Author

*E-mail: (W.L.) wmliu@mail.ipc.ac.cn, (P.W.) wangpf@mail.ipc.ac.cn.

Notes

The authors declare no competing financial interest.

■ ACKNOWLEDGMENTS

This work was supported by the NNSF of China (Grant Nos. 20903110, 61227008, 21073213, and 20673132) and the Main Direction Program of Knowledge Innovation of Chinese Academy of Sciences.

■ REFERENCES

(1) (a) Yuan, L.; Lin, W.; Zheng, K.; He, L.; Huang, W. *Chem. Soc. Rev.* **2013**, *42*, 622. (b) Schäferling, M. *Angew. Chem., Int. Ed.* **2012**, *51*, 3532. (c) Chan, J.; Dodani, S. C.; Chang, C. J. *Nat. Chem.* **2012**, *4*, 973.

(2) (a) Zheng, H.; Zhan, X.-Q.; Bian, Q.-N.; Zhang, X.-J. *Chem. Commun.* **2013**, *49*, 429. (b) Sun, Y.-Q.; Liu, J.; Lv, X.; Liu, Y.; Zhao, Y.;

Guo, W. *Angew. Chem., Int. Ed.* **2012**, *51*, 7634. (c) Chen, X.; Pradhan, T.; Wang, F.; Kim, J. S.; Yoon, J. *Chem. Rev.* **2012**, *112*, 1910.
(3) (a) Summerhayes, I. C.; Lampidis, T. J.; Bernal, S. D.; Nadakavukaren, J. J.; Nadakavukaren, K. K.; Shepherd, E. L.; Chen, L. B. *Proc. Natl. Acad. Sci. U.S.A.* **1982**, *79*, 5292. (b) Darzynkiewicz, Z.; Staianocoico, L.; Melamed, M. R. *Proc. Natl. Acad. Sci. U.S.A.* **1981**, *78*, 2383. (c) Johnson, L. V.; Walsh, M. L.; Chen, L. B. *Proc. Natl. Acad. Sci. U.S.A.* **1980**, *77*, 990.
(4) Shi, W.; Ma, H. *Chem. Commun.* **2012**, *48*, 8732.
(5) Kim, H. N.; Ren, W. X.; Kim, J. S.; Yoon, J. *Chem. Soc. Rev.* **2012**, *41*, 3210.
(6) Fan, J.; Hu, M.; Zhan, P.; Peng, X. *Chem. Soc. Rev.* **2013**, *42*, 29.
(7) (a) Yuan, L.; Lin, W.; Yang, Y.; Chen, H. *J. Am. Chem. Soc.* **2012**, *134*, 1200. (b) Kolmakov, K.; Belov, V. N.; Bierwagen, J.; Ringemann, C.; Müller, V.; Eggeling, C.; Hell, S. W. *Chem.—Eur. J.* **2010**, *16*, 158. (c) Weissleder, R.; Ntziachristos, V. *Nat. Med.* **2003**, *9*, 123.
(8) Qian, G.; Wang, Z. Y. *Chem.—Asian J.* **2010**, *5*, 1006.
(9) Karton-Lifshin, N.; Albertazzi, L.; Bendikov, M.; Baran, P. S.; Shabat, D. *J. Am. Chem. Soc.* **2012**, *134*, 20412.
(10) (a) Koide, Y.; Urano, Y.; Hanaoka, K.; Piao, W.; Kusakabe, M.; Saito, N.; Terai, T.; Okabe, T.; Nagano, T. *J. Am. Chem. Soc.* **2012**, *134*, 5029. (b) Koide, Y.; Urano, Y.; Hanaoka, K.; Terai, T.; Nagano, T. *J. Am. Chem. Soc.* **2011**, *133*, 5680.
(11) (a) Glancy, B.; Balaban, R. S. *Biochemistry* **2012**, *51*, 2959. (b) Lee, S.; Chen, X. *ChemBioChem* **2011**, *12*, 2120. (c) Abeliovich, A. *Nature* **2010**, *463*, 744.
(12) (a) Wallace, D. C. *Nat. Rev. Cancer* **2012**, *12*, 685. (b) Manji, H.; Kato, T.; Di Prospero, N. A.; Ness, S.; Beal, M. F.; Krams, M.; Chen, G. *Nat. Rev. Neurosci.* **2012**, *13*, 293. (c) Goldberg, J. A.; Guzman, J. N.; Estep, C. M.; Ilijic, E.; Kondapalli, J.; Sanchez-Padilla, J.; Surmeier, D. J. *Nat. Neurosci.* **2012**, *15*, 1414. (d) Zhou, R.; Yazdi, A. S.; Menu, P.; Tschopp, J. *Nature* **2011**, *469*, 221. (e) Blanco, F. J.; Rego, I.; Ruiz-Romero, C. *Nat. Rev. Rheumatol.* **2011**, *7*, 161.
(13) (a) Hoye, A. T.; Davoren, J. E.; Wipf, P.; Fink, M. P.; Kagan, V. E. *Acc. Chem. Res.* **2008**, *41*, 87. (b) Murphy, M. P.; Smith, R. A. J. *Annu. Rev. Pharmacol. Toxicol.* **2007**, *47*, 629.
(14) (a) Li, L.; Ge, J.; Wu, H.; Xu, Q.-H.; Yao, S. Q. *J. Am. Chem. Soc.* **2012**, *134*, 12157. (b) Qian, F.; Zhang, C.; Zhang, Y.; He, W.; Gao, X.; Hu, P.; Guo, Z. *J. Am. Chem. Soc.* **2009**, *131*, 1460. (c) Kim, Y. K.; Ha, H.-H.; Lee, J.-S.; Bi, X.; Ahn, Y.-H.; Hajar, S.; Lee, J.-J.; Chang, Y.-T. *J. Am. Chem. Soc.* **2009**, *132*, 576.
(15) Zhan, X.-Q.; Qian, Z.-H.; Zheng, H.; Su, B.-Y.; Lan, Z.; Xu, J.-G. *Chem. Commun.* **2008**, *44*, 1859.
(16) Frisch, M. J.; Trucks, G. W.; Schlegel, H. B.; Scuseria, G. E.; Robb, M. A.; Cheeseman, J. R.; Montgomery, J. A. Jr.; Vreven, T.; Kudin, K. N.; Burant, J. C.; Millam, J. M.; Iyengar, S. S.; Tomasi, J.; Barone, V.; Mennucci, B.; Cossi, M.; Scalmani, G.; Rega, N.; Petersson, G. A.; Nakatsuji, H.; Hada, M.; Ehara, M.; Toyota, K.; Fukuda, R.; Hasegawa, J.; Ishida, M.; Nakajima, T.; Honda, Y.; Kitao, O.; Nakai, H.; Klene, M.; Li, X.; Knox, J. E.; Hratchian, H. P.; Cross, J. B.; Bakken, V.; Adamo, C.; Jaramillo, J.; Gomperts, R.; Stratmann, R. E.; Yazyev, O.; Austin, A. J.; Cammi, R.; Pomelli, C.; Ochterski, J. W.; Ayala, P. Y.; Morokuma, K.; Voth, G. A.; Salvador, P.; Dannenberg, J. J.; Zakrzewski, V. G.; Dapprich, S.; Daniels, A. D.; Strain, M. C.; Farkas, O.; Malick, D. K.; Rabuck, A. D.; Raghavachari, K.; Foresman, J. B.; Ortiz, J. V.; Cui, Q.; Baboul, A. G.; Clifford, S.; Cioslowski, J.; Stefanov, B. B.; Liu, G.; Liashenko, A.; Piskorz, P.; Komaromi, I.; Martin, R. L.; Fox, D. J.; Keith, T.; Al-Laham, M. A.; Peng, C. Y.; Nanayakkara, A.; Challacombe, M.; Gill, P. M. W.; Johnson, B.; Chen, W.; Wong, M. W.; Gonzalez, C.; Pople, J. A. Gaussian, Inc., Wallingford CT, 2004.
(17) (a) Sommer, J. R.; Shelton, A. H.; Parthasarathy, A.; Ghiviriga, I.; Reynolds, J. R.; Schanze, K. S. *Chem. Mater.* **2011**, *23*, 5296. (b) Knight, T. E.; Goldstein, A. P.; Brennaman, M. K.; Cardolaccia, T.; Pandya, A.; DeSimone, J. M.; Meyer, T. J. *J. Phys. Chem. B* **2011**, *115*, 64. (c) Fenwick, O.; Sprafke, J. K.; Binas, J.; Kondratuk, D. V.; Di Stasio, F.; Anderson, H. L.; Cacialli, F. *Nano Lett.* **2011**, *11*, 2451.
(18) Arden-Jacob, J.; Frantzeskos, J.; Kemnitzer, N. U.; Zilles, A.; Drexhage, K. H. *Spectrochim. Acta, Part A* **2001**, *57*, 2271.
(19) Magde, D.; Brannon, J. H.; Cremers, T. L.; Olmsted, J. *J. Phys. Chem.* **1979**, *83*, 696.
(20) Leung, C. W. T.; Hong, Y.; Chen, S.; Zhao, E.; Lam, J. W. Y.; Tang, B. Z. *J. Am. Chem. Soc.* **2012**, *135*, 62.
(21) (a) Yu, H.; Xiao, Y.; Guo, H.; Qian, X. *Chem.—Eur. J.* **2011**, *17*, 3179. (b) Lin, W.; Yuan, L.; Cao, Z.; Feng, Y.; Song, J. *Angew. Chem., Int. Ed.* **2010**, *49*, 375.
(22) Chen, Y.-S.; Kuo, P.-Y.; Shie, T.-L.; Yang, D.-Y. *Tetrahedron* **2006**, *62*, 9410.
(23) Boyarskiy, V. P.; Belov, V. N.; Medda, R.; Hein, B.; Bossi, M.; Hell, S. W. *Chem.—Eur. J.* **2008**, *14*, 1784.
(24) Drexhage, K.-H.; Arden-Jacob, J.; Kemnitzer, N. *Amidopyrylium fluorescence dyes.* US 6737280, May 18, 2004.
(25) Kojima, H.; Hirotani, M.; Nakatsubo, N.; Kikuchi, K.; Urano, Y.; Higuchi, T.; Hirata, Y.; Nagano, T. *Anal. Chem.* **2001**, *73*, 1967.